A Family of $\Delta\Sigma$ Modulators With High Spur Immunity and Low Folded Nonlinearity Noise When Used in Fractional-N Frequency Synthesizers

Valerio Mazzaro, *Member, IEEE*, and Michael Peter Kennedy, *Fellow, IEEE*

***Abstract*— Phase locked loops for fractional frequency synthesis typically use Digital $\Delta\Sigma$ Modulators (DDSMs) as their divider controllers. Different types and configurations of DDSMs have been presented in the past which have distinctive characteristics in terms of spectral shaping of their quantization errors, spur immunity and implementation costs. This paper presents a family of DDSMs that have provably high spur immunity and low folded noise when used in fractional-N frequency synthesizers with polynomial nonlinearities.**

***Index Terms*— Frequency synthesizer, enhanced nonlinearity-induced noise performance (ENOP) digital delta-sigma modulator (DDSM), spurious tones, noise folding, nonlinearity.**

I. Introduction

PHASE locked loops (PLL) usually employ digital $\Delta\Sigma$ modulators (DDSM) in order to implement fractional frequency synthesis. The DDSM approximates the fractional part of the frequency multiplication factor by means of a time-varying integer-valued signal. The latter is used to control the instantaneous divide ratio of a multi-modulus divider (MMD) in the feedback path of the synthesizer. The integer approximation that is implemented by the DDSM inevitably introduces a quantization error. The accumulation of this quantization error leads to a time-varying phase error in the system.

The modulator should be designed so that the power spectral density (PSD) of the DDSM-related phase error in fractional-N mode does not degrade the phase noise performance of the synthesizer significantly relative to its integer-N counterpart. Relevant aspects of a modulator are the randomization and the spectral shaping of the quantization error [1]–[4]. In fact, it is desirable that the PSD of the DDSM-related phase error is devoid of idle tones and is high-pass shaped. This latter property is obtained via the design of the noise transfer function of the modulator; it is beneficial because the phase noise introduced by the modulator is subsequently low-pass filtered by the system's closed-loop transfer function. On the other hand, randomization of the quantization error is achieved using techniques that aim to increase the cycle length of the modulator and make it noiselike [5], [6].

Unfortunately, these techniques alone do not prevent the generation of DDSM-related spurious tones and low-frequency noise floor in a nonlinear synthesizer. In fact, the DDSM-related phase error interacts with nonlinearities that are present in the loop and both spurs and folded noise arise [7]–[11]. Many techniques have been developed to linearize the system [12]–[15]. While these attenuate the spurs and the folded noise, they do not eliminate them completely because a residual nonlinearity is inevitably present.

A different approach to improving the fractional spur-performance of charge-pump (CP) PLLs has been pursued by using the Successive Requantizer (SR) [16] and the Probability Modulator Redistributor (PMR) [17], [18]; these modify the statistical properties of the DDSM signal so that the distorted phase error signal does not produce spurs. In the case of the SR, it has been proven that this architecture has an output that is provably spur free when it is distorted by a specific polynomial nonlinearity. In a recent paper, it has been proven that MASH modulators also provide spur immunity for certain polynomial nonlinearities because of the statistical properties of the accumulated quantization error [19]. In particular, the higher the order of the MASH modulator, the higher is the order of the polynomial nonlinearity up to which the modulator is immune from spurs. However, just like the SR, as the order of the MASH DDSM increases, so does the level of folded noise that it introduces [20].

In this paper, we introduce a family of DDSMs, called Enhanced Nonlinearity-induced nOise Performance digital $\Delta\Sigma$ modulators (ENOP-DDSMs) which, like the SR, can achieve immunity to spurs for memoryless polynomial nonlinearities of up to a certain order. The flexibility of the architecture, underpinned by an analytical evaluation of the spurious behavior [21] and folded noise generation [20], allows one to design an ENOP-DDSM that achieves the same level of spur immunity that can be achieved by the best SRs and PMRs, but with a lower folded noise floor.

Manuscript received 31 January 2022; revised 29 June 2022; accepted 18 July 2022. Date of publication 10 August 2022; date of current version 26 October 2022. This work was supported in part by the Science Foundation Ireland under Grant 13/IA/1979 and Grant 20/FFP-A/8371 and in part by the Enterprise Ireland under Grant TC-2015-0019. This article was recommended by Associate Editor N. Krishnapura. *(Corresponding author: Valerio Mazzaro.)*

Valerio Mazzaro is with the School of Electrical and Electronic Engineering and the Microelectronic Circuits Centre Ireland, University College Dublin, Dublin 4, D04 V1W8 Ireland, and also with STMicroelectronics, 27100 Pavia, Italy (e-mail: valerio.mazzaro@ucdconnect.ie).

Michael Peter Kennedy is with the School of Electrical and Electronic Engineering and the Microelectronic Circuits Centre Ireland, University College Dublin, Dublin 4, D04 V1W8 Ireland (e-mail: peter.kennedy@ucd.ie).

Color versions of one or more figures in this article are available at https://doi.org/10.1109/TCSI.2022.3195659.

Digital Object Identifier 10.1109/TCSI.2022.3195659

This work is licensed under a Creative Commons Attribution 4.0 License. For more information, see https://creativecommons.org/licenses/by/4.0/

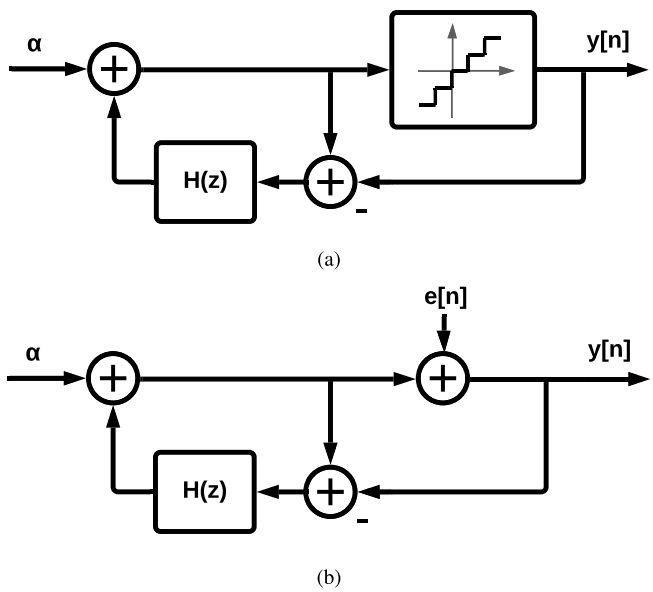

Fig. 1. (a) Block diagram of an error feedback modulator (EFM) and (b) its linearized model.

The paper is organized as follows. In Section II we give some background on the modulation noise introduced by the DDSM, and a method to evaluate the spur immunity. The structure of an ENOP-DDSM is described in detail in Section III, where a number of representative ENOP-DDSM configurations, which combine spur immunity with low folded noise, are presented. In Section IV, the spur immunity of these ENOP-DDSMs is analyzed. These results are confirmed by simulations in Section V. Finally, we draw our conclusions in Section VI.

II. Background

By definition, DDSMs coarsely quantize an over-sampled digital input signal. In the case of fractional frequency synthesizers, the ratio of the output frequency to the reference frequency, denoted N_{div}, can be expressed as $N_{int} + \alpha$, where N_{int} is the integer part of N_{div} and α is the fractional part. The latter, in turn, can be implemented as a ratio X/M, where X and M are, respectively, the integer-valued input word and the modulus of the modulator. The modulator introduces a quantization error, namely $e_q[n]$, while approximating the fractional value α with its quantized output $y[n]$, such that:

$$y[n] = \alpha + e_q[n]. \tag{1}$$

The statistical and spectral properties of the quantization error depend on the type and order of the modulator. Let us consider, for example, the error feedback modulator (EFM) shown in Fig. 1.

The signal $e[n]$ represents the error introduced by the quantizer. In particular, the accumulator-based digital quantizer implements a truncation and provides only integer values at its output. Therefore, the signal $e[n]$ only assumes values in the range $(-1, 0]$. The expression for the output of a generic single-quantizer DDSM in the Z-domain is given by [22]:

$$Y(z) = STF(z) \cdot X(z) + NTF(z) \cdot E(z), \tag{2}$$

where X(z) is the Z-transform of the generic input $x[n]$, $E(z)$ is the Z-transform of $e[n]$ and the functions $STF(z)$ and $NTF(z)$ are, respectively, the signal and noise transfer functions. In the case of the modulator presented in Fig. 1, $x[n]$ is equal to α and $STF(z)$ is equal to unity. On the other hand, the $NTF(z)$ is given by:

$$NTF(z) = 1 - H(z). \tag{3}$$

As mentioned before, the error $e[n]$ is high-pass shaped so that the quantization noise is moved out of band to be low pass filtered by the loop. Therefore, $H(z)$ is commonly designed such that the $NTF(z)$ is equal to $\left(1 - z^{-1}\right)^l$, where l represents the order of the modulator [4]. Doing so, the Z-transform of $e_q[n]$ may be expressed as:

$$E_q(z) = \left(1 - z^{-1}\right)^l E(z). \tag{4}$$

Eq. (1) illustrates that $e_q[n]$ is the error between the desired frequency ratio and the one implemented instantaneously in the system. Therefore, it represents the frequency error introduced by the modulator. Consequently, the accumulation of $e_q[n]$, denoted as $e_{acc}[n]$, contains information related to the phase error introduced into the loop by the DDSM [23]. From (4), the Z-transform of the accumulated quantization error is given by:

$$\begin{aligned} E_{acc}(z) &= \left(1 - z^{-1}\right)^{-1} E_q(z) \\ &= \left(1 - z^{-1}\right)^{l-1} E(z). \end{aligned} \tag{5}$$

Its expression in the time domain is given by:

$$e_{acc}[n] = \sum_{i=0}^{l-1} (-1)^i \binom{l-1}{i} e[n-i]. \tag{6}$$

Knowing the statistical and spectral characteristics of $e_{acc}[n]$ is fundamental to understanding the effect of the DDSM on the fractional-N frequency synthesizer. If the quantization error is sufficiently well randomized [5], [6], the PSD of e_{acc} is spur-free.

Fig. 2 shows a phase-domain model of the synthesizer under consideration. A real PLL inevitably experiences nonlinearities in the loop. For instance, in the case of CP-PLLs, the PFD/CP block typically exhibits a memoryless nonlinearity.[1]

The nonlinear PFD/CP has been modelled in Fig. 2 as a cascade of a dimensionless block that takes into account the nonlinearity and offset, followed by a linear PFD/CP. If the system is locked and there are no other sources of noise in the loop, the phase error experienced at the input of the phase frequency detector (PFD) can be expressed as:

$$\Delta\phi_{in}[n] = \frac{2\pi}{N_{div}} \left(e_{acc}[n-1] + \tau_{os}\right), \tag{7}$$

where $\frac{2\pi}{N_{div}}\tau_{os}$ is a phase offset that is introduced by the system and it is present in addition to the term in e_{acc}. Such a non-zero

[1]In general, a PFD/CP block exhibits both static and dynamic mismatches [10], [24]. However, previous work has shown that some typical dynamic mismatches can be approximated by a memoryless nonlinear function (see, for example [8], [11]).

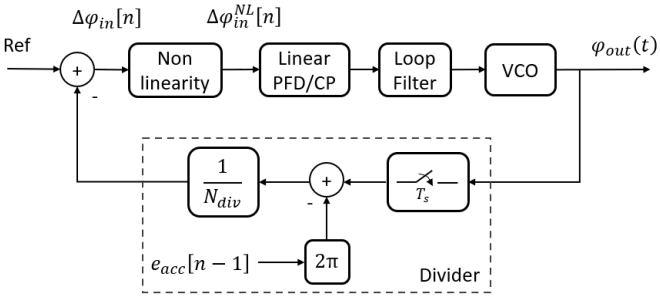

Fig. 2. Phase-domain model of a PLL [23], whose nonlinear PFD/CP block has been partitioned into a memoryless nonlinearity followed by a linear PFD/CP block.

value of τ_{os} can be caused by the presence of nonlinearities in the system or by offsets that are voluntarily introduced into the loop, such as CP bleed current [25].

From the results in (5) and (7), one may deduce that, when $l > 1$, the DDSM-related phase noise $\Delta\phi_{in}$, which is derived from e_{acc}, is high-pass shaped and, therefore, its low frequency component is suppressed. However, interaction of this phase error with the nonlinearity leads to the generation of extra noise that is manifest as spurious tones and an elevated noise floor [3].

In Fig. 2, we denote by $\Delta\phi_{in}^{NL}[n]$ the input phase error after distortion by the nonlinearity. Then, the noise generated by the nonlinearity can by studied by analyzing the PSD of $\Delta\phi_{in}^{NL}$, denoted by $S_{\Delta\phi_{in}^{NL}}$. Let us introduce the nonlinear function $\mathcal{N}(\cdot)$, and express $\Delta\phi_{in}^{NL}[n]$ as a function of $e_{acc}[n]$, namely:

$$\Delta\phi_{in}^{NL}[n] = \frac{2\pi}{N_{div}}\mathcal{N}\left(e_{acc}[n-1] + \tau_{os}\right), \tag{8}$$

where we define:

$$e_{acc}^{NL}[n] = \mathcal{N}\left(e_{acc}[n] + \tau_{os}\right). \tag{9}$$

It is worth reiterating that, in a type-II PLL, the value of τ_{os} is such that $E\left[e_{acc}^{NL}[n]\right] = 0$.

In recent work [21], Donnelly and Kennedy have presented a semi-analytical method to predict the spurious behavior of a fractional-N frequency synthesizer once the nonlinearity is specified. This is obtained by calculating the periodic component of the noise generated by the nonlinearity, the so-called Periodic Nonlinearity Noise (PNN). It is pointed out in [21] that, for any $n \in \mathbb{N}$, $e_{acc}[n]$ lies on a set of continuous sawtooth tracks, denoted by $\tau_m(t)$, which are defined as:

$$\tau_m(t) = m - (\alpha t \mod 1) \tag{10}$$

where $t \in \mathbb{R}$ and $m \in \mathbb{Z}$. Moreover, the samples of the accumulated quantization error are not uniformly distributed over these tracks. Instead, the probability distribution, denoted by $P(\cdot)$, depends on the modulator. Then, the distorted accumulated quantization error, $e_{acc}^{NL}[n]$, lies on a set of distorted tracks which are defined as:

$$\hat{\tau}_m{}^{NL}(t) = \mathcal{N}(\tau_m(t) + \tau_{os}). \tag{11}$$

Therefore, the locations and the amplitudes of the nonlinearity-induced spurs can be predicted by calculating the Fourier transform of the PNN, which is defined as [21]:

$$PNN[n] = \sum_m \hat{\tau}_m{}^{NL}(n) P\left(\tau_m(n)\right), \tag{12}$$

where $\hat{\tau}_m^{NL}(n) = \hat{\tau}_m^{NL}(t)|_{t=n}$ and $\tau_m(n) = \tau_m(t)|_{t=n}$.

The synthesizer does not experience fractional spurs due to $\mathcal{N}(\cdot)$ if the PNN is constant and equal to zero. Recently, it has been proven, by means of the PNN, that MASH-based synthesizers exhibit spur immunity for certain polynomial nonlinearities [19]. In the following sections, we will use the PNN and the method developed in [19] to analyze the level of spur immunity of the ENOP-DDSM family for a given order of polynomial nonlinearity $\mathcal{N}(\cdot)$.

TABLE I
SIMULATION MODEL PARAMETERS

Parameter	Value
f_{ref}	122.88 MHz
I_{CPnom}	1.5 μA
Loop filter gain	1.65×10^{11}
Loop filter zero (ω_z)	3.77×10^4 rad/s
Loop filter poles ($\omega_{p1}, \omega_{p2}, \omega_{p3}$)	$0, 1.93 \times 10^6 \pm j1.9 \times 10^6$ rad/s
K_{VCO}	6 MHz/V
N_{int}	41
LSB dither	1st-order shaped
M	2^{20}

III. ENOP-DDSMs

A. Examples

ENOP-DDSMs are characterized by being able to achieve high spur immunity while simultaneously minimizing the folded noise resulting from nonlinear distortion. An example is given in Fig. 3, where the simulated phase noise performance of both a linear and a nonlinear fractional frequency synthesizer are compared for four different divider controller architectures, namely a MASH 1-1-1, a MASH 1-1-1-1, a second order Successive Requantizer (SR2) and an ENOP-DDSM, in the presence of a cubic nonlinearity.[2]

These results have been obtained via closed-loop phase-domain simulations of the CP-PLL model shown in Fig. 2. The transfer function of the loop filter is

$$L(s) = \frac{1.65 \cdot 10^{11} \cdot (1 + 2.65 \cdot 10^{-5}s)}{1 + 5.26 \cdot 10^{-7}s + 1.38 \cdot 10^{-13}s^2}[\Omega] \tag{13}$$

The model parameters are summarized in Table I. The reference noise and physical divider, VCO, PFD and CP noise are assumed zero. The closed loop bandwidth is approximately 300 kHz.

In the case of a linear synthesizer, shown in Fig. 3(a), the output phase noise is given by the DDSM noise filtered by the closed loop transfer function of the PLL. This condition exposes big differences between the different architectures of modulators. The SR and the ENOP P1 have the larger noise contributions that are quite similar.

[2]In order to improve the randomization of the quantization error we consider only odd values for X. Moreover, for each modulator but the SR2, we have added a first order shaped LSB dither to randomize further the quantization error generated by the modulators.

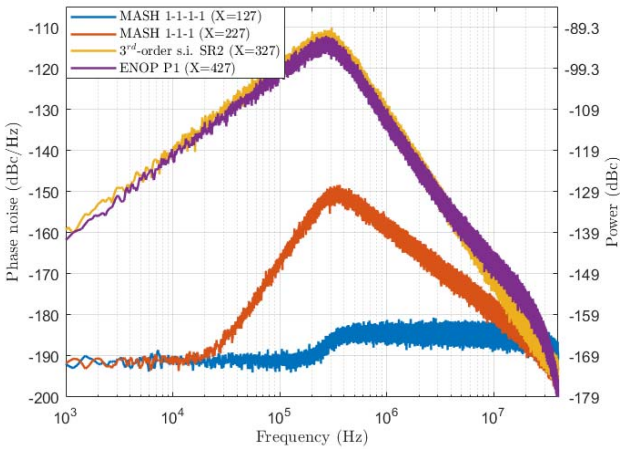

(a)

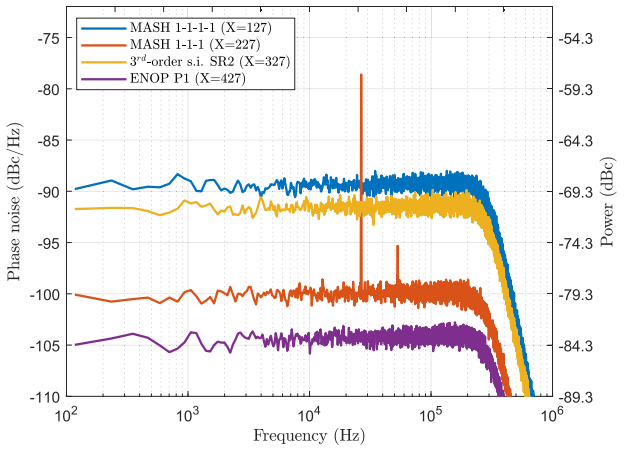

(b)

Fig. 3. Comparison of the simulated phase noise of (a) a linear fractional-N PLL characterized in Table I for different DDSMs: MASH 1-1-1-1, 3rd-order spur immune (s.i.) SR2 [26], MASH 1-1-1 and an ENOP-DDSM (P1 of Table IV) and (b) in the case of a third-order nonlinearity $\mathcal{N}(x) = x + 0.02x^2 + 0.01x^3$. The P1 ENOP (in purple) is both spur-free and exhibits the lowest folded noise floor.

The situation changes substantially when the system is nonlinear. Note that the MASH 1-1-1 (shown in brick red in Fig. 3) has a folded noise floor at -100 dBc/Hz and exhibits a strong fractional spur at $\approx$ 14.9 kHz ($= \frac{X}{M} f_{ref}$). Many commercial fractional-N synthesizers use MASH 1-1-1 divider controllers and, therefore, exhibit spurs of this type.

The MASH 1-1-1-1 (in blue) is provably spur free for this nonlinearity and therefore does not exhibit a spur [19]. However, its folded noise floor is at approximately -90 dBc/Hz. The SR2[3] (in yellow) is provably spur free but it too has an elevated noise floor [26]. The ENOP-DDSM (in purple) is also provably spur free, as we will show, and its folded noise contribution at -104 dBc/Hz is the best of the four examples. The performance results are summarized in Table II.

[3]With SR2, we mean a second order Successive Requantizer. In particular, the SR2 of this example is the one described in [26, Fig. 6 and eq. (31)].

TABLE II

SIMULATED PERFORMANCE FOR THE THIRD-ORDER POLYNOMIAL IN FIG.3(B)

DDSM	Worst spur (dBc)	In-band noise (dBc/Hz)
MASH 1-1-1-1	N/A	-90
MASH 1-1-1	-58	-100
3rd-order s.i. SR2	N/A	-92
ENOP P1	N/A	-104

TABLE III

SIMULATED PERFORMANCE FOR THE SEVENTH-ORDER NONLINEARITY IN FIG.4(B)

DDSM	Worst spur (dBc)	In-band noise (dBc/Hz)
MASH 1-1-1-1	-52	-86
MASH 1-1-1	-57	-101
3rd-order s.i. SR2	-62	-89
ENOP P5	N/A	-94

In this example, we have shown that the ENOP P1 has the best noise and spur performance of the architectures considered when the system is nonlinear.

Another example is considered in Fig. 4, where the MASH 1-1-1, MASH 1-1-1-1 and SR2 are compared with another ENOP DDSM variant, denoted by ENOP P5, in the case of a seventh-order nonlinearity. As before, the noise performances are compared first without and then with the nonlinearity. Note that the ENOP P5 has a DDSM noise profile that closely follows that of the MASH 1-1-1 up to 1 MHz in the linear case, as shown in Fig. 4(a). Furthermore, in the presence of the nonlinearity, shown in Fig. 4(b), the ENOP P5 is the only DDSM that does not produce any spur. In fact, as we will show later, the ENOP P5 allows one to achieve spur-free operation in the case of polynomial nonllinearities up to order seven.

While the folded noise generated by the ENOP P5 is larger than that of the MASH 1-1-1, it is considerably lower than the other two solutions. These performance results are summarized in Table III.

We will show in the following sections that an ENOP-DDSM can be designed to prioritize spur-immunity, to minimize folded noise or to provide a compromise between the two. This is possible because the DDSM-related noise generated by the nonlinearity can be predicted in advance once information about $e_{acc}[n]$ is known.

B. Architecture

The ENOP-DDSM can be implemented with an EFM structure, as shown in Fig. 1. The governing equation is (2) where the $STF(z)$ is equal to unity. The $NTF(z)$ of an lth order ENOP-DDSM has the form:

$$NTF(z) = \left(1 - z^{-1}\right)\left(1 + \sum_{i=1}^{l-1} c_i z^{-i}\right), \tag{14}$$

where l represents the order of the ENOP-DDSM. According to (3), the desired $NTF(z)$ in (14) can be obtained by

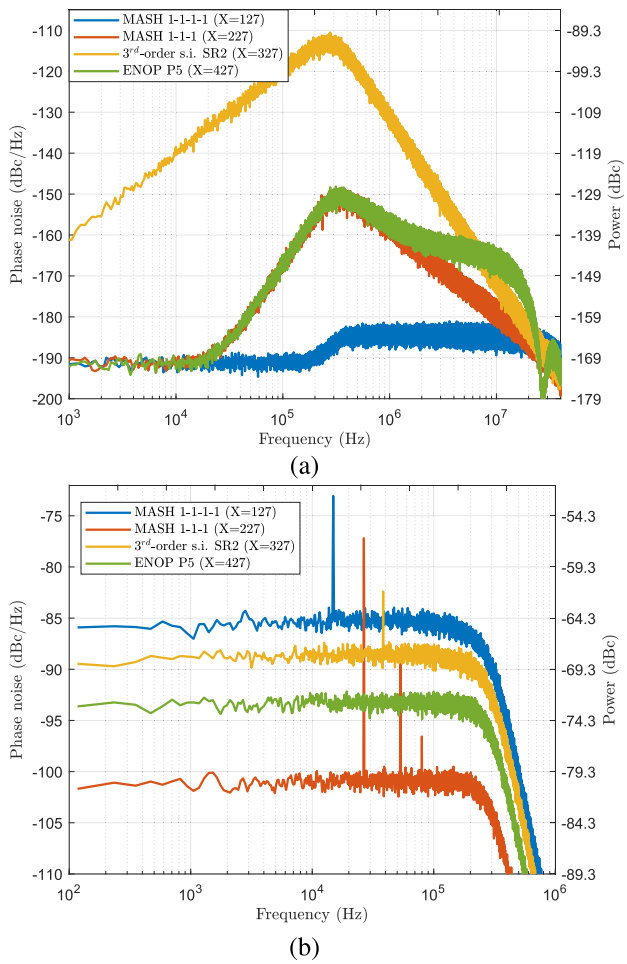

Fig. 4. Comparison of the simulated phase noise of (a) a linear fractional-N PLL characterized in Table I for different DDSMs: MASH 1-1-1-1, 3rd-order spur immune (s.i.) SR2 [26], MASH 1-1-1 and an ENOP-DDSM (P5 of Table IV) and (b) in the case of a seventh-order nonlinearity $\mathcal{N}(x) = x - 0.02x^2 + 0.01x^3 + 0.003x^4 - 0.01x^5 - 0.0003x^6 + 0.0006x^7$. Different values of X have been used for the four DDSMs in order to offset their spur positions. Although the MASH 1-1-1 has a lower noise floor, only the P5 ENOP (in green) is spur-free.

choosing:

$$H(z) = 1 - NTF(z) = z^{-1} - \left(1 - z^{-1}\right)\sum_{i=1}^{l-1} c_i z^{-i}. \tag{15}$$

With this transfer function, the modulator will produce an accumulated quantization error whose Z-transform is equal to:

$$E_{acc}(z) = E(z)\left(1 + \sum_{i=1}^{l-1} c_i z^{-i}\right), \tag{16}$$

where $E(z)$ is the Z-transform of the error $e[n]$ generated by the quantizer. One can express $e_{acc}[n]$ as:

$$e_{acc}[n] = e[n] + \sum_{i=1}^{l-1} c_i e[n-i]. \tag{17}$$

For the remainder of this work we will assume that every coefficient c_i in (14) is integer valued. This is not necessary but it simplifies the implementation.

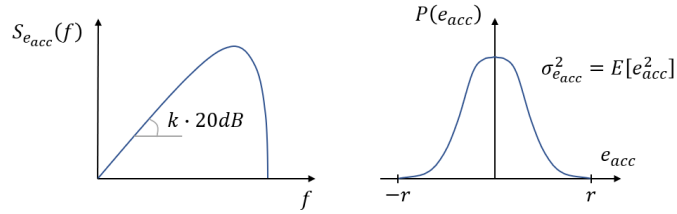

Fig. 5. Example of PSD and pdf of e_{acc} showing the respective parameters: k, r and $\sigma^2_{e_{acc}}$, where $E[e_{acc}] = 0$.

At this point, we list the key parameters that determine the performance of an ENOP-DDSM. These are as follows:

- l: the order of the modulator.
- k: the order of low-frequency high-pass shaping of the accumulated quantization error.
- r: the half width of the range of the accumulated quantization error.
- p: the order of polynomial nonlinearities up to which the accumulated quantization error is immune from spurs.
- $\sigma^2_{e_{acc}}$: the variance of the accumulated quantization error.

Some of these parameters (k, r, $\sigma^2_{e_{acc}}$) are illustrated schematically in Fig. 5.

The order of the modulator, l, sets the number of coefficients c_i which, in turn, determine the signal e_{acc} generated by the modulator. Therefore, the value of l determines the number of degrees of freedom available when designing the ENOP-DDSM which is, in principle, $(l-1)$. The larger is l the greater is the number of delay elements (registers) that are needed for implementing the block $H(z)$ in (15). Consequently, a larger l comes with a higher hardware cost.

As pointed out previously, it is important to high-pass shape the PSD of e_{acc} so that the low-frequency component of the modulation-related phase noise is suppressed. The order of high-pass shaping at low frequencies, k, is determined by the number of solutions of $E_{acc}(z) = 0$ at $z = 1$. As a consequence, the value of k sets constraints on the values that can be assumed by c_i. In other words, the number of degrees of freedom for designing the modulator decreases to $(l-1-k)$. This means that, for a given l, the greater is k the less room will be left for designing the modulator so that other performance characteristics are met.

In the frequency synthesizer application, the value of k has to be greater than or equal to one. When more aggressive high-pass shaping is demanded, for example when a wide synthesizer bandwidth is required and/or a low reference frequency is employed, the choice of $k = 2$ is suitable. Higher values for k would require a more aggressive roll-off of the loop filter in the synthesizer to suppress the resulting high-frequency noise component.

C. Spur Immunity

One of the most important parameters of the ENOP-DDSM is p; this determines the level of spur immunity of the modulator. Since the modulator has to be designed such that $k \geq 1$, the coefficients c_i are chosen so that:

$$1 + \sum_{i=1}^{l-1} c_i = 0 \tag{18}$$

Therefore, the signal e_{acc} has a range that is symmetric about zero. In particular, we introduce the parameter r, which is the smallest integer such that:

$$-r < e_{acc} < r \tag{19}$$

Moreover, since $e[n] \in (-1, 0]$, from (17), (18) and the definition of r, one can show that:

$$r = \frac{1 + \sum_{i=1}^{l-1} |c_i|}{2} \tag{20}$$

Familier and Galton have proven that the maximum attainable order p of spurious tone immunity for polynomial nonlinearities is $(2r - 1)$ and that there exist quantizers which are immune to spurs up to order $(2r - 1)$ [27], [28].[4] This implies that the optimal property with respect to spur immunity in the presence of a polynomial nonlinearity is given by:

$$p_{opt} = 2r - 1 \tag{21}$$

It is interesting to note that the optimal condition for spur immunity can be obtained only for *odd* values of p.

D. Folded Noise

The result in (21) suggests that e_{acc} must have a larger range in order to achieve spur immunity to higher order polynomial nonlinearities. However, a wider range for the accumulated quantization error would lead to stronger interaction with the nonlinearity and, qualitatively, a higher level of folded noise. The level of the noise floor can be predicted using methods such as those presented in [11], [20] and [29]. For the sake of simplicity, in this paper we will estimate the severity of the generated folded noise with $\sigma^2_{e_{acc}}$, the variance of the accumulated quantization error. In fact, it has been reported that the level of the in-band folded noise floor scales qualitatively with $\sigma^2_{e_{acc}}$ [11].[5] Therefore, the value of $\sigma^2_{e_{acc}}$ provides a rough estimate of the folded noise performance of a modulator.

If we assume that $e[n]$ is a uniform independent and identically distributed (i.i.d.) stochastic process then, considering (17) and (18), the variance of e_{acc} becomes:

$$\sigma^2_{e_{acc}} = \frac{1}{12}\left(1 + \sum_{i=1}^{l-1} c_i^2\right). \tag{22}$$

This assumption about $e[n]$ is only an approximation; however, it allows one to obtain an accurate estimate of the statistical properties of e_{acc} [20]. We will use this assumption later in the paper for evaluating the probability distribution of e_{acc}.

Eq. (22) shows that, in order to minimize the variance of e_{acc}, each non-zero integer coefficient c_i has to have an absolute value equal to one. This, according to the expressions (20) and (22), gives:

$$\sigma^2_{e_{acc},min} = \frac{r}{6} \tag{23}$$

[4]It is worth remarking that we use a different nomenclature compared to [27], [28]. The accumulated quantization error e_{acc}, its single-sided range r and the order of spur immunity p are denoted in those works by, respectively, $t[n]$, N_t and h_t. Therefore, for a given N_t, the maximum value of h_t is expressed as $(2N_t - 1)$.

[5]It is important to remark that the folded noise level is not a bijective function of $\sigma^2_{e_{acc}}$. The former depends also on the spectrum of e_{acc}.

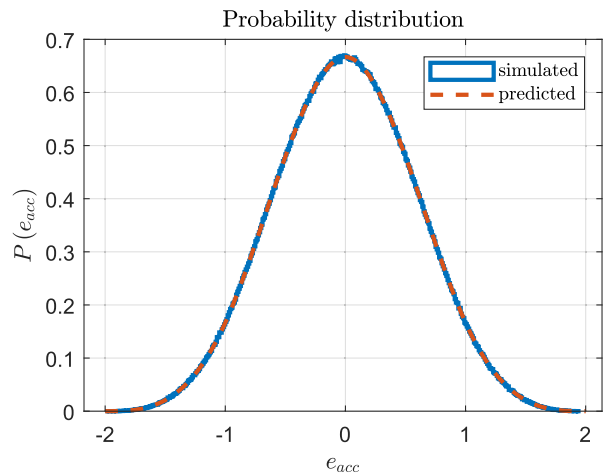

Fig. 6. Predicted and simulated probability distribution of e_{acc} in the case of P1 ENOP-DDSM; $r = 2$.

In summary, for a given value of r, the maximum achievable order of spur immunity is equal to $(2r - 1)$. Moreover, once r is fixed, the minimum value of $\sigma^2_{e_{acc}}$ with integer coefficients is equal to $r/6$ and this is obtained when all the non-zero coefficients c_i have magnitudes equal to one.

Table IV shows simulation results for seven sample ENOP-DDSMs with $r = 2$, 3, 4 and 5. The corresponding values of $\sigma^2_{e_{acc}}$ are 1/3, 1/2, 2/3 and 5/6, respectively. We will next show that these architectures are also optimal in the sense that they achieve $p = p_{opt}$.

IV. Analysis of Spur Immunity via Symbolic Calculation of PNN

In this section we analyze the spur immunity for the ENOP-DDSMs proposed in Table IV by using the PNN. Then, we confirm the properties of spur immunity through behavioral simulations of the nonlinear frequency synthesizer. As previously presented, the PNN represents a valuable tool to determine the immunity from spurs of a given modulator. In fact, if the PNN is constant and equal to zero, the system does not experience spurs [19]. From the work presented in [21], the PNN (defined by (12)) can be evaluated for a given modulator and nonlinearity once the probability distribution function of e_{acc}, denoted by $P(\cdot)$, is known. The latter can be predicted if we make the assumption that $e[n]$ is a uniform and i.i.d. stochastic process [30], [31]; further details are provided in Appendix A.

We know that the hypothesis made about $e[n]$ is not strictly true; nevertheless, under typical conditions it leads to accurate predictions for $P(\cdot)$. For example, let us consider the case of a P1 ENOP-DDSM. Following the procedure presented in Appendix A, one can evaluate the probability distribution function of e_{acc} from (31), obtaining:

$$P(x) = \begin{cases} \frac{1}{6}\left(4 - 6x^2 + 3|x|^3\right) & \text{if } \ 0 \le |x| \le 1 \\ \frac{1}{6}\left(2 - |x|\right)^3 & \text{if } \ 1 \le |x| \le 2 \\ 0 & \text{elsewhere} \end{cases} \tag{24}$$

The predicted probability distribution is compared to simulation results in Fig. 6.

TABLE IV
EXAMPLES OF RELEVANT CONFIGURATIONS OF ENOP ΔΣ MODULATORS

Architecture	l	k	r	p_{opt}	$NTF(z)$	$\sigma^{2*}_{e_{acc}}$	p
ENOP P1	5	1	2	3	$\left(1-z^{-1}\right)\left(1-z^{-1}-z^{-2}+z^{-4}\right)$	≈ 0.333	3
ENOP P2	6	1	3	5	$\left(1-z^{-1}\right)\left(1-z^{-1}-z^{-2}+z^{-3}-z^{-4}+z^{-5}\right)$	≈ 0.5	5
ENOP P3	7	2	3	5	$\left(1-z^{-1}\right)\left(1-z^{-1}+z^{-2}-z^{-3}-z^{-4}+z^{-6}\right)$	≈ 0.5	5
ENOP P4	8	1	4	7	$\left(1-z^{-1}\right)\left(1-z^{-1}-z^{-2}+z^{-3}-z^{-4}+z^{-5}-z^{-6}+z^{-7}\right)$	≈ 0.667	7
ENOP P5	9	2	4	7	$\left(1-z^{-1}\right)\left(1-z^{-1}-z^{-2}+z^{-3}-z^{-4}+z^{-5}+z^{-7}-z^{-8}\right)$	≈ 0.667	7
ENOP P6	10	1	5	9	$\left(1-z^{-1}\right)\left(1-z^{-1}-z^{-2}+z^{-3}-z^{-4}+z^{-5}-z^{-6}+z^{-7}-z^{-8}+z^{-9}\right)$	≈ 0.833	9
ENOP P7	11	2	5	9	$\left(1-z^{-1}\right)\left(1-z^{-1}-z^{-2}+z^{-3}-z^{-4}+z^{-5}-z^{-6}+z^{-7}+z^{-8}-z^{-10}\right)$	≈ 0.833	9

* The $\sigma^2_{e_{acc}}$ has been evaluated numerically through simulations.

Notice that the simulated distribution $P(e_{acc})$ closely matches the analytical prediction. This confirms the validity of the approximation made about e_{acc}. The predictions of $P(e_{acc})$ for the other architectures of ENOP-DDSMs presented in Table IV are provided in Appendix A.

Equation (24) allows one to evaluate the PNN for the P1 architecture once the nonlinearity is specified. In particular, let us consider the case of P1 interacting with a generic third order polynomial nonlinearity, expressed as $\mathcal{N}(x) = \sum_{i=0}^{3} a_i x^i$. From the definitions in (10)–(12), and considering the expression of the predicted $P(\cdot)$ (24), one can show that:

$$PNN[n] = a_0 + a_1\tau_{os} + a_2\left(\frac{1}{3} + \tau_{os}^2\right) + a_3\left(\tau_{os} + \tau_{os}^3\right), \tag{25}$$

which is independent of n and is therefore constant. Moreover, because of the locking condition of a type-II PLL, τ_{os} is valued so that $E\left[PNN\left[n\right]\right] = 0$. Therefore, the PNN expressed in (25) is equal to zero, which means that the system does not experience fractional spurs in the case of polynomial nonlinearities up to the third order[6] when a P1 ENOP-DDSM is used. This confirms that the level of spur immunity p for the P1 ENOP-DDSM equals the optimal value p_{opt} shown in Table IV. Repeating a similar PNN analysis for the other proposed architectures yields the characteristics of spur immunity listed in Table IV, as shown in Appendix B. In each case, the P1–P7 ENOP-DDSMs achieve a level of spur immunity equal to p_{opt} and are optimal in the sense of Familier and Galton [28].

Concluding, the architectures listed in Table IV match the condition of best spur immunity and the lowest folded noise. In fact, they are both p-optimal and exhibit minimal $\sigma^2_{e_{acc}}$.

V. VALIDATION BY BEHAVIORAL SIMULATION OF PLL

In this section we validate the performance of representative ENOP-DDSMs in the frequency synthesizer application through behavioral simulations of a nonlinear charge pump (CP) PLL where the divider controller is implemented with the NTFs listed in Table IV. The simulations were performed using a phase domain closed-loop model implemented in MATLAB [23]. The parameters of the simulated system are listed in Table I. The physical noise of the VCO, PFD and CP, as well as the reference noise are assumed zero.

[6]Eq. (25) shows that the P1 is immune from spurs in the case of a third order nonlinearity. However, it is easy to notice that in the case of polynomial nonlinearities with order lower than three, one or more coefficients a_i in (25) would be equal to zero, leading to a PNN which is still independent of n. Therefore, we can say that the immunity holds *up to* and including third order.

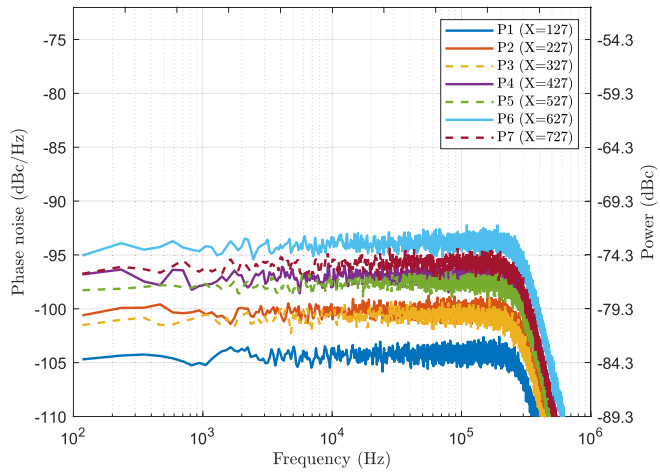

Fig. 7. Simulated phase noise in the case of cubic nonlinearity ($\mathcal{N}(x) = x + 0.02x^2 + 0.01x^3$) for the different ENOP-DDSMs.

In the simulations we assume zero reference noise and physical divider, VCO, PFD and CP noise. This does not represent what happens in a real circuit; however, it allows one to visualize better in isolation the effects of the interaction between the quantization noise and the nonlinearity, the so-called "mathematical noise", for the different cases of ENOP-DDSMs. Furthermore, first-order shaped LSB dither is applied to the modulator to ensure that the quantization error is sufficiently randomized [5], while an odd value for the input X is chosen to mitigate against possible horn spurs [32].[7]

A. Third-Order Polynomial

We first consider the case where the synthesizer exhibits a third-order polynomial nonlinearity. The results of the simulations are shown in Fig. 7. Different values of X have been used for the DDSMs so that their spurs (if any) do not overlap in the figures.

With a MASH 1-1-1 DDSM, a fixed integer boundary spur would be expected at $\frac{X}{M} f_{ref} \approx 14.9$ kHz. From Table IV, all of the listed ENOP-DDSMs are expected to provide spur immunity in the presence of third-order nonlinearities. This is confirmed by the simulations. Note that no spurs are present in any of the ENOP-DDSMs.

It is worth noticing also that the level of folded noise varies between the different modulators. This is to be expected, since $\sigma^2_{e_{acc}}$ varies as well. In fact, as discussed in Section III, the folded noise floor scales with $\sigma^2_{e_{acc}}$. Therefore, we expect that two different modulators that share the same value of

[7]Together, the odd input and shaped LSB dither are sufficient to make $e[n]$ approximately uniform and i.i.d.

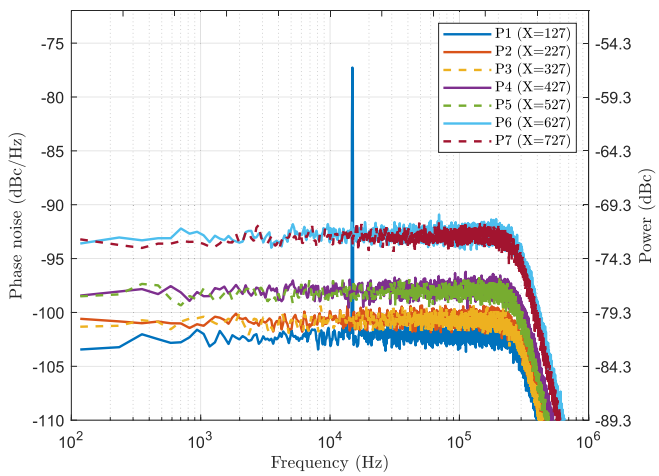

Fig. 8. Simulated phase noise in the case of fifth-order nonlinearity ($\mathcal{N}(x) = x + 0.04x^2 + 0.03x^3 - 0.01x^4 - 0.005x^5$) for the different ENOP-DDSMs.

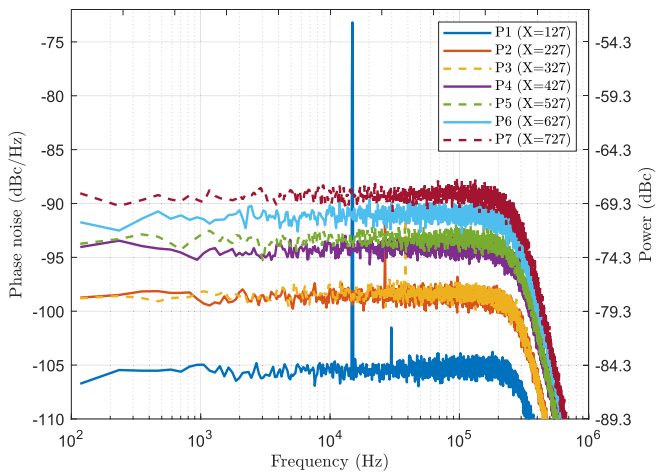

Fig. 9. Simulated phase noise in the case of seventh-order nonlinearity ($\mathcal{N}(x) = x - 0.02x^2 + 0.01x^3 + 0.003x^4 - 0.01x^5 - 0.0003x^6 + 0.0006x^7$) for the different ENOP-DDSMs. Synthesizers with P1, P2 and P3 all exhibit spurs; P4–P7 do not.

$\sigma^2_{e_{acc}}$ should generate similar levels of folded noise. Moreover, the latter increases as $\sigma^2_{e_{acc}}$ gets bigger. This is confirmed in Fig. 7, where P1, which has $\sigma^2_{e_{acc}} = 1/3$, contributes the lowest excess noise, while P6 and P7, which have $\sigma^2_{e_{acc}} = 5/6$, have the highest.

B. Fifth-Order Polynomial

Next, we consider the case where the nonlinearity is a fifth-order polynomial. From the analysis in Section III, we predict spurious tones for the P1 ENOP-DDSM and spur immunity in the other cases. This is confirmed by the simulation results in Fig. 8. In particular, note the integer boundary spur at ≈ 14.9 kHz in Fig. 8.

Similar considerations to the previous case can be made for the folded noise: P1 is the best while P6 and P7 are the worst.

C. Seventh-Order Polynomial

Lastly, we consider the case of a seventh-order polynomial nonlinearity. This example confirms that P4, P5, P6 and P7 ENOP-DDSMs are spur immune up to seventh-order polynomial nonlinearities. This is shown in Fig. 9. Notice that the cases of P1, P2 and P3 exhibit spurs since their p is less than 7. Note also that the level of the folded noise grows as the variance of e_{acc} increases.

It should be clear at this point that the ENOP-DDSMs can provide different trade-offs between the order of spur rejection and the in-band noise floor, depending on the choice of NTF. Empirically, the higher is the spur immunity, the larger will be the folded noise. It follows that, depending on the performance one wishes to prioritize, one NTF might suit better than the others.

VI. Conclusion

In this paper, we have presented a family of $\Delta\Sigma$ modulators which can be designed to be optimal in the sense of Familier and Galton in terms of spurious tone immunity for polynomial nonlinearities. An analytical method has been presented to predict both the level of spur immunity and the folded noise floor. The predictions have been confirmed by simulation. The results show the potential of ENOP-DDSMs to match the state of the art performance in terms of spur immunity. Moreover, with the same level of spur immunity, ENOP-DDSMs have a lower hardware complexity and can outperform the prior art in terms of folded noise.

Appendix A
Prediction of e_{acc} Probability Distribution

In previous publications [19], [21], it has been shown that the spurious behavior resulting from the interaction between the quantization error and system nonlinearities can be predicted by the PNN. Evaluation of the PNN requires knowledge of the probability distribution function of the accumulated quantization error, denoted by $P(\cdot)$. In a recent paper, this function has been derived empirically for some MASH modulators [19]. In this appendix, we provide a method to predict $P(\cdot)$ for a generic ENOP-DDSM, under the hypothesis that $e[n]$ is an independent and identically uniformly distributed $\mathcal{U}(-1, 0)$ stochastic process.

In [30], the author evaluates the probability distribution of a multivariate random function by applying the *variable transformation theorem* [31]. In particular, consider a random variable Y which is a function of k independent random variables with arbitrary probability distributions:

$$Y = g\left(X_1, X_2, \ldots, X_k\right), \tag{26}$$

considering that such a function can be expressed explicitly in terms of any of the independent variables (i.e. X_1), so that:

$$X_1 = g_1^{-1}\left(Y, X_2, \ldots, X_k\right), \tag{27}$$

with n_1 possible solutions. Then, the probability density function of Y is [30]:

$$\begin{aligned} f_Y(y) = &\int_{x_k=-\infty}^{x_k=\infty} \cdots \int_{x_3=-\infty}^{x_3=\infty} \int_{x_2=-\infty}^{x_2=\infty} \prod_{j=2}^{k} \left(f_{X_j}\left(x_j\right) dx_j\right) \\ &\times \sum_{i=1}^{n_1} f_{X_1}\left(g_{1,i}^{-1}\left(y, x_2, x_3, \ldots, x_k\right)\right) \\ &\times \left|\frac{\partial g_{1,i}^{-1}\left(y, x_2, x_3, \ldots, x_k\right)}{\partial y}\right| \end{aligned} \tag{28}$$

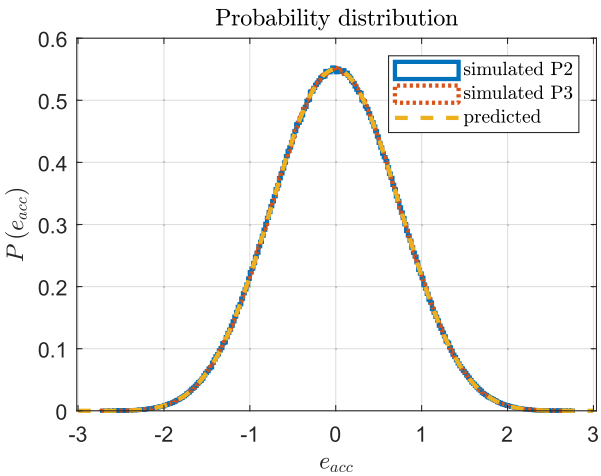

Fig. 10. Predicted and simulated probability distribution of e_{acc} in the cases of P2 and P3 ENOP-DDSM; $r = 3$.

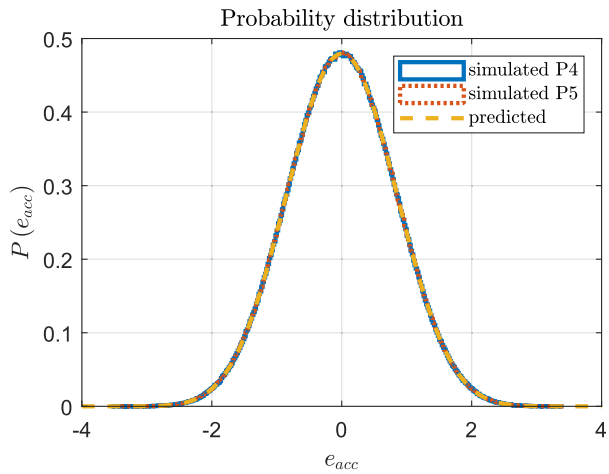

Fig. 11. Predicted and simulated probability distribution of e_{acc} in the cases of P4 and P5 ENOP-DDSM; $r = 4$.

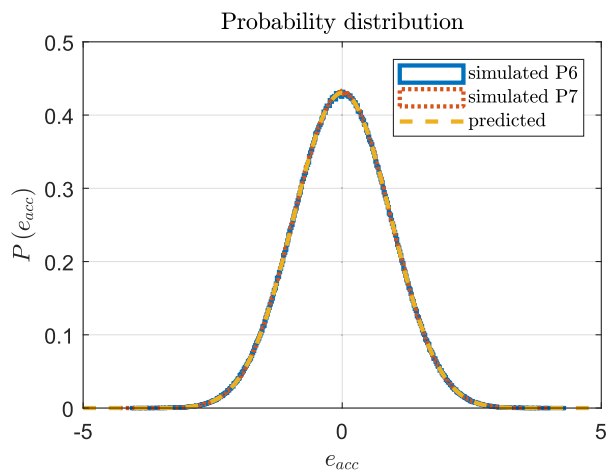

Fig. 12. Predicted and simulated probability distribution of e_{acc} in the cases of P6 and P7 ENOP-DDSM; $r = 5$.

Assuming that $e[n]$ is a uniform and i.i.d. stochastic process, each pair of signals $e[n-i]$, $e[n-j]$ is independent for every $i \neq j$. According to this assumption and the expression in (16), one can notice that the e_{acc} of an ENOP-DDSM is a function of l independent random variables, where l is the order of the modulator. For the sake of simplicity, let us denote each random variable $e[n-j]$ by e_j. Doing so, we can represent e_{acc} as:

$$e_{acc} = e_0 + c_1 e_1 + c_2 e_2 + \ldots + c_{l-1} e_{l-1}, \tag{29}$$

It is clear that the function in (29) can be expressed explicitly in terms of any e_j with only one solution. Let us consider for instance e_0:

$$e_0 = e_{acc} - c_1 e_1 - c_2 e_2 + \ldots - c_{l-1} e_{l-1}. \tag{30}$$

Furthermore, let us remember that each e_j is valued only in the range $(-1, 0]$. Then, similarly to (28), we can evaluate the probability density function of e_{acc} as:

$$f_{e_{acc}}(y) = \int_{x_{l-1}=-1}^{x_{l-1}=0} \cdots \int_{x_2=-1}^{x_2=0} \int_{x_1=-1}^{x_1=} \prod_{j=1}^{l-1} \left(f_{e_j}\left(x_j\right) dx_j \right) \times f_{e_0}\left(y - c_1 x_1 - c_2 x_2 + \ldots - c_{l-1} x_{l-1}\right) \tag{31}$$

This function is also denoted in the paper by $P(\cdot)$.[8]

The evaluation of the probability distribution of e_{acc} for the architecture P1 is already discussed in Section IV. Following the same procedure for architectures P2 and P3, one would obtain that the predicted $P(\cdot)$ is given by:

$$P(x) = \begin{cases} \frac{1}{60}\left(33 - 30x^2 + 15x^4 - 5|x|^5\right) & \text{if } 0 \leq |x| \leq 1 \\ \frac{51+75|x|-210x^2+150|x|^3-45x^4+5|x|^5}{120} & \text{if } 1 \leq |x| \leq 2 \\ \frac{1}{120}(3-|x|)^5 & \text{if } 2 \leq |x| \leq 3 \\ 0 & \text{elsewhere} \end{cases} \tag{32}$$

Similarly, the pairs of architectures P4 and P5 also share a common $P(\cdot)$ which is expressed in (33), as shown at the top of the next page. Finally, the probability distribution of e_{acc}, for cases P6 and P7 is given in (34), as shown at the top of the next page. The predicted probability distributions shown in (32)–(34) are compared to simulation results in Figs. 10, 11 and 12, respectively. Notice that all the simulated distributions $P(e_{acc})$ closely match the predictions, confirming the validity of the approximation made about e_{acc}.

[8]For each configuration we describe, eq. (31) has been evaluated using Mathematica to determine $P(\cdot)$.

Appendix B
Evaluation of p for Representative ENOP-DDSM Architectures

In Section IV, we discussed the possibility of predicting the spur immunity of a DDSM for a given nonlinearity, through the evaluation of the PNN. Moreover, we have analyzed and proven the level of spur immunity p listed in Table IV for the case of P1. In this Appendix, we extend the analysis to the other architectures of ENOP-DDSMs presented in Table IV.

Let us consider first the P2 and P3 ENOP-DDSM architectures. The PNN can be evaluated from the definitions in (10)–(12) and the expression for the predicted $P(\cdot)$ given in (24). If we assume a generic fifth-order nonlinearity expressed as

$$P(x) = \begin{cases} \frac{2416-1680x^2+560x^4-140x^6+35|x|^7}{5040} & \text{if } 0 \le |x| \le 1 \\ \frac{2472-392|x|-504x^2-1960|x|^3+2520x^4-1176|x|^5+252x^6-21|x|^7}{5040} & \text{if } 1 \le |x| \le 2 \\ \frac{-1112+12152|x|-19320x^2+13720|x|^3-5320x^4+1176|x|^5-140x^6+7|x|^7}{5040} & \text{if } 2 \le |x| \le 3 \\ \frac{1}{5040}(4-|x|)^7 & \text{if } 3 \le |x| \le 4 \\ 0 & \text{elsewhere} \end{cases} \tag{33}$$

$$P(x) = \begin{cases} \frac{78095-44100x^2+11970x^4-2100x^6+315x^8-63|x|^9}{181440} & \text{if } 0 \le |x| \le 1 \\ \frac{77990+945|x|-47880x^2+8820|x|^3-1260x^4+13230|x|^5-10920x^6+3780|x|^7-630x^8+42|x|^9}{181440} & \text{if } 1 \le |x| \le 2 \\ \frac{108710-137295|x|+228600x^2-313740|x|^3+240660x^4-107730|x|^5+29400x^6-4860|x|^7+450x^8-18|x|^9}{181440} & \text{if } 2 \le |x| \le 3 \\ \frac{-668315+2382615|x|-3085740x^2+2128140|x|^3-896490x^4+243810|x|^5-43260x^6+4860|x|^7-315x^8+9|x|^9}{362880} & \text{if } 3 \le |x| \le 4 \\ \frac{1}{362880}(5-|x|)^9 & \text{if } 4 \le |x| \le 5 \\ 0 & \text{elsewhere} \end{cases} \tag{34}$$

$\mathcal{N}(x) = \sum_{i=0}^{5} a_i x^i$, we obtain:

$$\begin{aligned} PNN[n] = {} & a_0 + a_1\tau_{os} + a_2\left(\frac{1}{2}+\tau_{os}^2\right) + a_3\left(\frac{3}{2}\tau_{os}+\tau_{os}^3\right) \\ & + a_4\left(\frac{7}{10}+3\tau_{os}^2+\tau_{os}^4\right) \\ & + a_5\left(\frac{7}{2}\tau_{os}+5\tau_{os}^3+\tau_{os}^5\right) \end{aligned} \tag{35}$$

The resulting PNN is independent of n. As discussed in Section IV, this means that the system does not experience fractional spurs and, therefore, the P2 and P3 ENOP-DDSMs provide a level of spur immunity p equal to 5, as anticipated in Table IV.

Then, we analyze the cases of P4 and P5 architectures. They share the same probability distribution function for e_{acc}, which is given in (33). Following the same procedure for evaluating the PNN and considering a seventh-order nonlinearity, $\mathcal{N}(x) = \sum_{i=0}^{7} a_i x^i$, one finds that:

$$\begin{aligned} & PNN[n] \\ & = a_0 + a_1\tau_{os} + a_2\left(\frac{2}{3}+\tau_{os}^2\right) + a_3(2\tau_{os}+\tau_{os}^3) \\ & \quad + a_4\left(\frac{19}{15}+4\tau_{os}^2+\tau_{os}^4\right) + a_5\left(\frac{19}{5}\tau_{os}+\frac{20}{3}\tau_{os}^3+\tau_{os}^5\right) \\ & \quad + a_6\left(\frac{80}{21}+19\tau_{os}^2+10\tau_{os}^4+\tau_{os}^6\right) + a_7\left(\frac{80}{3}\tau_{os}\right. \\ & \quad \left. + \frac{133}{3}\tau_{os}^3+14\tau_{os}^5+\tau_{os}^7\right), \end{aligned} \tag{36}$$

which is again independent of n. This result confirms that P4 and P5 architectures achieve $p = 7$.

Lastly, we consider the cases of P6 and P7 ENOP-DDSMs. In Table IV, we stated that these architectures achieve spur immunity to polynomials up to ninth order. To prove this, let us consider a nonlinearity $\mathcal{N}(x) = \sum_{i=0}^{9} a_i x^i$. Then, we evaluate the PNN using the expression of $P(\cdot)$ given in (34). Doing so, one obtains:

$$\begin{aligned} & PNN[n] \\ & = a_0 + a_1\tau_{os} + a_2\left(\frac{5}{6}+\tau_{os}^2\right) + a_3\left(\frac{5}{2}\tau_{os}+\tau_{os}^3\right) \\ & \quad + a_4\left(2+5\tau_{os}^2+\tau_{os}^4\right) + a_5\left(10\tau_{os}+\frac{25}{3}\tau_{os}^3+\tau_{os}^5\right) \\ & \quad + a_6\left(\frac{215}{28}+30\tau_{os}^2+\frac{25}{2}\tau_{os}^4+\tau_{os}^6\right) + a_7\left(\frac{215}{4}\tau_{os}\right. \\ & \quad \left. + 70\tau_{os}^3+\frac{35}{2}\tau_{os}^5+\tau_{os}^7\right) + a_8\left(\frac{713}{18}+215\tau_{os}^2+140\tau_{os}^4\right. \\ & \quad \left. + \frac{70}{3}\tau_{os}^6+\tau_{os}^8\right) + a_9\left(\frac{713}{2}\tau_{os}+645\tau_{os}^3+252\tau_{os}^5\right. \\ & \quad \left. + 30\tau_{os}^7+\tau_{os}^9\right) \end{aligned} \tag{37}$$

This shows that the PNN is constant and confirms that architectures P6 and P7 are immune from spurious tones in the case of polynomial nonlinearities with order up to nine. It should be clear that the method can be extended to higher orders albeit with more terms in the expressions for $P(x)$ and $PNN[n]$.

REFERENCES

[1] M. Kozak and I. Kale, "A pipelined noise shaping coder for fractional-N frequency synthesis," *IEEE Trans. Instrum. Meas.*, vol. 50, no. 5, pp. 1154–1161, Oct. 2001.

[2] M. J. Borkowski, T. A. D. Riley, J. Hakkinen, and J. Kostamovaara, "A practical Δ-Σ modulator design method based on periodical behavior analysis," *IEEE Trans. Circuits Syst. II, Exp. Briefs*, vol. 52, no. 10, pp. 626–630, Oct. 2005.

[3] B. De Muer and M. Steyaert, *CMOS Fractional-N Synthesizers: Design for High Spectral Purity and Monolithic Integration*, vol. 724. New York, NY, USA: Springer-Verlag, 2006. [Online]. Available: https://link.springer.com/book/10.1007/b101854

[4] S. Pavan, R. Schreier, and G. C. Temes, *Understanding Delta-Sigma Data Converters*. Hoboken, NJ, USA: Wiley, 2017.

[5] S. Pamarti and I. Galton, "LSB dithering in MASH delta–sigma D/A converters," *IEEE Trans. Circuits Syst. I, Reg. Papers*, vol. 54, no. 4, pp. 779–790, Apr. 2007.

[6] K. Hosseini and M. P. Kennedy, *Minimizing Spurious Tones in Digital Delta-Sigma Modulators*. New York, NY, USA: Springer, 2011. [Online]. Available: https://link.springer.com/book/10.1007/978-1-4614-0094-3

[7] B. De Muer and M. S. Steyaert, "A CMOS monolithic $\Delta\Sigma$-controlled fractional-N frequency synthesizer for DCS-1800," *IEEE J. Solid-State Circuits*, vol. 37, no. 7, pp. 835–844, Jul. 2002.

[8] H. Hedayati, B. Bakkaloglu, and W. Khalil, "Closed-loop nonlinear modeling of wideband $\Sigma\Delta$ fractional-N frequency synthesizers," *IEEE Trans. Microw. Theory Techn.*, vol. 54, no. 10, pp. 3654–3663, Oct. 2006.

[9] W. Khalil, H. Hedayati, B. Bakkaloglu, and S. Kiaei, "Analysis and modeling of noise folding and spurious emission in wideband fractional-N synthesizers," in *Proc. IEEE Radio Freq. Integr. Circuits Symp.*, Jun. 2008, pp. 291–294.

[10] F. Bizzarri, A. M. Brambilla, and S. Callegari, "On the mechanisms governing spurious tone injection in fractional PLLs," *IEEE Trans. Circuits Syst. II, Exp. Briefs*, vol. 64, no. 11, pp. 1267–1271, Nov. 2017.

[11] H. Arora, N. Klemmer, J. C. Morizio, and P. D. Wolf, "Enhanced phase noise modeling of fractional-N frequency synthesizers," *IEEE Trans. Circuits Syst. I, Reg. Papers*, vol. 52, no. 2, pp. 379–395, Feb. 2005.

[12] S. E. Meninger and M. H. Perrott, "A 1-MHz bandwidth 3.6-GHz 0.18-μm CMOS fractional-N synthesizer utilizing a hybrid PFD/DAC structure for reduced broadband phase noise," *IEEE J. Solid-State Circuits*, vol. 41, no. 4, pp. 966–980, Apr. 2006.

[13] L. Zhang *et al.*, "A hybrid spur compensation technique for finite-modulo fractional-N phase-locked loops," *IEEE J. Solid-State Circuits*, vol. 44, no. 11, pp. 2922–2934, Nov. 2009.

[14] E. Temporiti, G. Albasini, I. Bietti, R. Castello, and M. Colombo, "A 700-KHz bandwidth $\Sigma\Delta$ fractional synthesizer with spurs compensation and linearization techniques for WCDMA applications," *IEEE J. Solid-State Circuits*, vol. 39, no. 9, pp. 1446–1454, Sep. 2004.

[15] C.-W. Yao *et al.*, "A 14-nm 0.14-ps_{rms} fractional-N digital PLL with a 0.2-ps resolution ADC-assisted coarse/fine-conversion chopping TDC and TDC nonlinearity calibration," *IEEE J. Solid-State Circuits*, vol. 52, no. 12, pp. 3446–3457, Dec. 2017.

[16] E. Familier and I. Galton, "Second and third-order successive requantizers for spurious tone reduction in low-noise fractional-N PLLs," in *Proc. IEEE Custom Integr. Circuits Conf. (CICC)*, Apr. 2017, pp. 1–4.

[17] Y. Donnelly *et al.*, "4.48-GHz fractional-N frequency synthesizer with spurious-tone suppression via probability mass redistribution," *IEEE Solid-State Circuits Lett.*, vol. 2, no. 11, pp. 264–267, Nov. 2019.

[18] H. Park, C. Hwang, T. Seong, Y. Lee, and J. Choi, "A 365 fs_{rms}-jitter and -63 dBc-fractional spur 5.3 GHz-ring-DCO-based fractional-N DPLL using a DTC second/third-order nonlinearity cancelation and a probability-density-shaping $\Delta\Sigma$M," in *IEEE Int. Solid-State Circuits Conf. (ISSCC) Dig. Tech. Papers*, vol. 64, Feb. 2021, pp. 442–444.

[19] V. Mazzaro and M. P. Kennedy, "Spur immunity in MASH-based fractional-N CP-PLLs with polynomial nonlinearities," *IEEE Trans. Circuits Syst. I, Reg. Papers*, vol. 68, no. 6, pp. 2295–2306, Jun. 2021.

[20] V. Mazzaro and M. P. Kennedy, "Folded noise prediction in nonlinear fractional-N frequency synthesizers," *IEEE Trans. Circuits Syst. I, Reg. Papers*, vol. 68, no. 10, pp. 4038–4048, Oct. 2021.

[21] Y. Donnelly and M. P. Kennedy, "Prediction of phase noise and spurs in a nonlinear fractional-N frequency synthesizer," *IEEE Trans. Circuits Syst. I, Reg. Papers*, vol. 66, no. 11, pp. 4108–4121, Nov. 2019.

[22] R. Schreier *et al.*, *Understanding Delta-Sigma Data Converters*, vol. 74. Piscataway, NJ, USA: IEEE Press, 2005.

[23] M. H. Perrott, M. D. Trott, and C. G. Sodini, "A modeling approach for fractional-N frequency synthesizers allowing straightforward noise analysis," *IEEE J. Solid-State Circuits*, vol. 37, no. 8, pp. 1028–1038, Sep. 2002.

[24] D. Biswas and T. K. Bhattacharyya, "Spur reduction architecture for multiphase fractional PLLs," *IET Circuits, Devices Syst.*, vol. 13, no. 8, pp. 1169–1180, Nov. 2019.

[25] B. Razavi, *Design of Analog CMOS Integrated Circuits*, 1st ed. New York, NY, USA: McGraw-Hill, 2001.

[26] E. Familier and I. Galton, "Second and third-order noise shaping digital quantizers for low phase noise and nonlinearity-induced spurious tones in fractional-N PLLs," *IEEE Trans. Circuits Syst. I, Reg. Papers*, vol. 63, no. 6, pp. 836–847, Jun. 2016.

[27] E. Familier and I. Galton, "A fundamental limitation of DC-free quantization noise with respect to nonlinearity-induced spurious tones," *IEEE Trans. Signal Process.*, vol. 61, no. 16, pp. 4172–4180, Aug. 2013.

[28] E. Familier, C. Venerus, and I. Galton, "A class of quantizers with DC-free quantization noise and optimal immunity to nonlinearity-induced spurious tones," *IEEE Trans. Signal Process.*, vol. 61, no. 17, pp. 4270–4283, Sep. 2013.

[29] B. Razavi, "An alternative analysis of noise folding in fractional-N synthesizers," in *Proc. IEEE Int. Symp. Circuits Syst. (ISCAS)*, 2018, pp. 1–4.

[30] H. Hernandez, "Multivariate probability theory: Determination of probability density functions," ForsChem Res., Medellin, Colombia, Rep. 13, 2017.

[31] G. Casella and R. L. Berger, *Statistical Inference*. Boston, MA, USA: Cengage Learning, 2021.

[32] V. Mazzaro and M. P. Kennedy, "Mitigation of 'horn spurs' in a MASH-based fractional-N CP-PLL," *IEEE Trans. Circuits Syst. II, Exp. Briefs*, vol. 67, no. 5, pp. 821–825, May 2020.

Valerio Mazzaro (Member, IEEE) was born in Salerno, Italy, in 1991. He received the B.Sc. and M.Sc. degrees in electronic engineering from the Università di Napoli Federico II, Naples, Italy, in 2014 and 2017, respectively. He is currently pursuing the Ph.D. degree with University College Dublin, Dublin, Ireland. In 2022, he joined STMicroelectronics, Pavia, Italy. His research interests include, frequency synthesizers, digital delta-sigma modulators, and phase-locked loops.

Michael Peter Kennedy (Fellow, IEEE) received the B.E. degree in electronics from the National University of Ireland, Dublin, in 1984, the M.S. and Ph.D. degrees from the University of California at Berkeley (UC Berkeley), Berkeley, in 1987 and 1991, respectively, and the D.Eng. degree from the National University of Ireland in 2010. He has worked as a Design Engineer with Philips Electronics, a Postdoctoral Research Engineer at the Electronics Research Laboratory, UC Berkeley, and a Professeur Invité at the Federal Institute of Technology Lausanne (EPFL), Switzerland. From 1992 to 2000, he was on the Faculty of the Department of Electronic and Electrical Engineering, University College Dublin (UCD), Dublin, Ireland, where he has taught electronic circuits and computer-aided circuit analysis and directed the Undergraduate Electronics Laboratory. In 2000, he joined University College Cork (UCC), Cork, Ireland, as a Professor and the Head of the Department of Microelectronic Engineering. He was the Founding Director of the Ireland's Microelectronics Industry Design Association in 2001. He was the Dean of the Faculty of Engineering, UCC, from 2003 to 2005, and the Vice-President for research from 2005 to 2010. He returned to UCD as a Professor of microelectronic engineering in 2017, where he is currently the Head of electronic engineering, School of Electrical and Electronic Engineering. He has been the Scientific Director of the Microelectronic Circuits Centre, Ireland, since 2010. He has taught courses on nonlinear dynamics and delta-sigma modulation in China, England, Greece, Hungary, Italy, South Korea, Spain, Switzerland, and USA. He has over 400 publications in the area of nonlinear circuits. His research interests are in the simulation, analysis, and design of nonlinear dynamical systems for applications in communications and signal processing. He was made an IEEE Fellow in 1998 for his contributions to the study of neural networks and nonlinear dynamics. He was elected to membership of the Royal Irish Academy (RIA) in 2004, served as a RIA Policy and International Relations Secretary from 2012 to 2016, and the President from 2017 to 2020. He was the Vice-President for Region 8 of the IEEE Circuits and Systems Society (CASS) from 2005 to 2007. He has served on the IEEE Fellows Committee, the IEEE Gustav Robert Kirchhoff Award Committee, and the IEEE Technical Field Awards Council. He was a recipient of the 1991 Best Paper Award from the *International Journal of Circuit Theory and Applications* and the Best Paper Award from the European Conference on Circuit Theory and Design in 1999. He was also awarded the IEEE Third Millennium Medal, the IEEE Circuits and Systems Society Golden Jubilee Medal in 2000, and the Inaugural Parson's Medal for Engineering Sciences by RIA in 2001. He has served as an Associate Editor for the IEEE TRANSACTIONS ON CIRCUITS AND SYSTEMS from 1993 to 1995 and from 1999 to 2004. He was a CASS Distinguished Lecturer from 2012 to 2013 and the Chair of the CASS Distinguished Lecturer Program in 2017 to 2020.